JET-P(96)43

The Effect of Finite Sheath Conductivity on the Interchange Instability in the SOL

W Kerner, A Nassigh[1], O Pogutse.

JET Joint Undertaking, Abingdon, Oxfordshire, OX14 3EA, UK.
[1] Dipartimento di Fisica, Universita di Milano, via Celoria 16, 20133 Milano, Italy.

Preprint of a submitted for publication in
Plasma Physics and Controlled Fusion

ABSTRACT

A linear analysis of MHD instabilities driven by the combined effects of unfavourable curvature and the pressure gradient is performed in the scrape-off layer of a limiter configuration. The dispersion relation of fast growing (electromagnetic) modes is derived by means of both analytical and numerical techniques. The growth rate dependence on the sheath resistivity and the magnetic shear is investigated. Perturbations are not completely stabilised by conducting end walls due to finite sheath conductivity. Modes develop into ideal ballooning modes as the plasma beta increases. The comparison of their behaviour to resistive ballooning modes shows that in most cases of interest the plasma stability is determined by the electromagnetic modes. As a consequence a new dependence of the instability growth rate on the plasma parameters is found, where the key parameter is the density close to the end plates. Results given here can be applied to a single-null divertor configuration.

1. INTRODUCTION

The scrape-off layer (SOL) is the thin (several gyroradii wide) region surrounding the last closed surface of a tokamak, either in limiter or divertor configurations. Understanding the nature of turbulence inside the SOL region is commonly considered a key issue in the explanation of important features in tokamak physics, such as the L-H transition, the occurrence of ELMs and the dependence of the SOL width on plasma parameters. SOL plasmas are characterised by open field lines, so that the theoretical investigation of SOL stability considerably differs from the analysis of the central region. Interchange and drift instabilities have been singled out among other modes characteristic of open field line systems as the most likely to be responsible for the SOL plasma turbulence [1-9].

In the present work we carry out a linear analysis of high mode number interchange instabilities. It is generally believed that the magnetic field stress prevents any plasma displacement when the ratio of the pressure and the magnetic field energy is below a critical value β_{cr}. According to this picture of the instability, only slow resistive modes can develop if the plasma beta is below the threshold value. Nedospasov, however, pointed out that electromagnetic modes driven by finite sheath conductivity are unstable at any value of the SOL beta [1]. These modes have been investigated in several theoretical works [2-5,10-14]. This paper continues the investigations of the previous work [12] in a more realistic geometry.

A detailed analysis of resistive ballooning modes has been proposed recently in Ref. [15]. It however takes into account only electrostatic modes. In this paper we apply the balloning formalism to the analysis of electromagnetic modes. We show that instabilities with a growth rate of the same order as ideal modes can develop with little field line bending, due to the

presence of a plasma-wall interface. In addition, we describe the growth rate dependence on sheath conductivity and magnetic configuration parameters. Modes described here transform smoothly into ideal ballooning modes localised on the low field side of the SOL as the plasma beta increases.

We refer to a magnetic configuration with a toroidal limiter placed on the bottom of the torus. This particular configuration has been chosen with the objective getting some insight on how modes behave in a single-null divertor configuration, like the present JET configuration. At this stage of the work we avoid the algebraic complexity which arises if we take into account the X-point in the poloidal magnetic field.

This paper is organised as follows. In Section 2 we describe the model used in the stability analysis. In Sec. 3 we derive some approximate dispersion relations for different limits of the plasma parameters. Sec. 4 is devoted to the numerical analysis of the problem. Finally, Sec. 5 contains a discussion of the results.

2. MODEL EQUATIONS

The relevant features of the interchange instability are derived in the framework of the single-fluid MHD model described in Refs. [16-17]. Magnetic field fluctuations parallel to the unperturbed field are assumed to be negligible compared to the equilibrium field. Consequently, only fluctuations in the perpendicular direction are considered and the electromagnetic field is described by means of the two scalars φ and $A_{||}$ (electrostatic potential and parallel component of the vector potential). The perpendicular current density $\boldsymbol{j}_{\perp}$ is determined by momentum balance, while the perturbation of the parallel component $\delta j_{||}$ (here and in the following perturbed quantities are denoted by δ) is determined by Ohm's law. The perpendicular motion is assumed to be given by the electric drift $\boldsymbol{v}_E = c\, \boldsymbol{b} \times \nabla\, \delta\varphi / B$, where $\boldsymbol{b}$ is an unit vector along the equilibrium magnetic field $\boldsymbol{B}$. In order to describe the main features of the instability, the parallel plasma motion and the effects due to finite ion drift frequency are not included in the model. These effects will not influence the qualitative picture of the modes drawn here, but may affect considerably the quantitative evaluation of the growth rate of the instability.

We are interested in the study of the evolution of perturbations characterised by a perpendicular wavelength much smaller than the pressure gradient length $x_0 = |\nabla p_0 / p_0|^{-1}$. Based on this assumption, we consider in the linearised fluid equations only the leading terms in the ordering $k_{\perp} x_0 >> 1$.

With this approximation the charge conservation and the parallel component of the Ohm's law read [18]

$$-\frac{\partial}{\partial t}\,\frac{c^2}{4\pi c_A^2}\,\nabla_{\perp}^2 \delta\varphi + c\,\nabla\,\delta p \cdot \nabla \times \left(\frac{\mathbf{b}}{B}\right) + \nabla_{||}\delta j_{||} = 0 \qquad (1)$$

$$\frac{\delta j_{\parallel}}{\sigma} = -\nabla_{\parallel}\delta\varphi - \frac{1}{c}\frac{\partial}{\partial t}\delta A_{\parallel} + \frac{1}{en}\nabla_{\parallel}\delta p \tag{2}$$

where $c_A = B / \sqrt{4\pi\rho}$ is the Alfvèn velocity, σ is the parallel Spitzer conductivity and, for simplicity, we assumed $\delta p_e = \delta p_i$. The pressure perturbation is related to the plasma motion by the following relation.

$$\frac{\partial}{\partial t}\delta p + \mathbf{v}_E \cdot \nabla p_0 = 0 \tag{3}$$

The set of Eqs. (1-3) is closed by the parallel component of the Ampère's law.

$$\mathbf{b}\cdot\nabla\times\nabla\times\left(\delta A_{\parallel}\,\mathbf{b}\right) = \frac{4\pi}{c}\delta j_{\parallel} \tag{4}$$

For the description of the equilibrium magnetic field in the SOL region we use a circular cross-section and an axisymmetric field $\boldsymbol{B} = B_0R_0/R\,(r/Rq\,\boldsymbol{e}_\theta + \boldsymbol{e}_\phi)$ in the conventional toroidal coordinate system (r, θ, ϕ) shown in Fig. 1. Here R_0 is the magnetic axis radius, $R = R_0 - r\cos\theta$, B_0 is the value of the magnetic field on the magnetic axis and q is the safety factor.

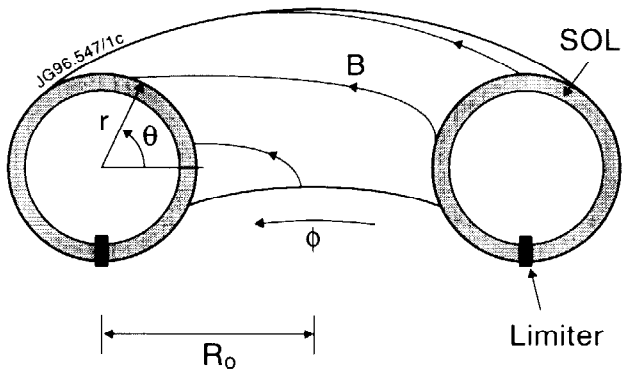

Fig.1: Coordinate system used in the problem.

Perturbed quantities in Eqs. (1-4) are written in the following form.

$$\delta \mathrm{f} = \tilde{\mathrm{f}}(r,\theta)e^{i\mathrm{S}(r,\theta,\phi)-i\omega t} \tag{5}$$

Here the frequency of the perturbation ω is in general complex and the Eikonal S is given by [19]

$$\mathrm{S} = n\left(\phi - \int_{\theta_0}^{\theta} q\,d\theta'\right) \tag{6}$$

where $n >> 1$ is the toroidal number of the perturbation and we introduce the parameter θ_0, i.e. the "origin" of the perturbation. It will be determined by maximising the growth rate, given by the imaginary part γ of the frequency [19].

To first order in n, Eq. (3) gives the relation between the pressure perturbation and the fluctuating electrostatic potential φ (here and in the following the tildes introduced in Eq. (5) are dropped).

$$\omega \frac{p}{p_0} = \frac{c T_0 k_\theta}{e B x_0} \frac{e\varphi}{T_0} \tag{7}$$

Here the poloidal wave number of the perturbation $k_\theta = nq/r$ has been introduced and T_0 is the equilibrium temperature (assumed for simplicity equal for ions and electrons).

To leading order in n, the system (1-4) is recast in the following second order ODE [18].

$$\frac{c_A^2}{L_{\|}} \frac{\partial}{\partial\theta}\left[\frac{k_\perp^2}{(\omega + i\omega_m) L_{\|}} \frac{\partial}{\partial\theta}\right]\varphi + \left[\omega k_\perp^2 + \frac{\omega_g^2}{\omega} k_\theta^2 \hat{G}\right]\varphi = 0 \tag{8}$$

Here $k_\perp^2 = k_\theta^2\left[1 + \hat{s}^2(\theta - \theta_0)^2\right]$ is the perpendicular wave number, the parameter $\hat{s} = \frac{r}{q}\frac{dq}{dr}$ denotes the magnetic shear, $\hat{G} = -2\left[\hat{s}(\theta - \theta_0)\sin\theta + \cos\theta\right]$ is the field line curvature operator, $L_{\|} = Rq$. Furthermore, two characteristic frequencies of the problem are introduced

$$\omega_g = \frac{c_s}{\sqrt{R x_0}} \tag{9}$$

$$\omega_m = k_\perp^2 D_m \tag{10}$$

where $c_s = \sqrt{T_0/m_i}$ is the sound speed and $D_m = c^2/4\pi\sigma$ is the magnetic diffusion coefficient.

Following Refs. [8,14], the boundary conditions of Eq. (8) are determined by the sheath physics. Neglecting density and temperature perturbations, the current density flowing through the sheath is related to the fluctuations of the electrostatic potential at the plasma side of the sheath by the following relations.

$$j_{\|}\Big|_{\substack{out \\ in}} = \pm e n^{ed} c_s^{ed} \frac{e\delta\varphi}{T^{ed}} \tag{11}$$

Here numerical factors of order one are omitted, n^{ed}, c_s^{ed} and T^{ed} are respectively the density, the sound speed and the temperature at the plasma side of the sheath. The labels "in" and "out" refer to the inner and the outer sides of the limiter. In the chosen coordinate system the inner and the outer plate are located at $\theta = -\pi/2$ and $\theta = 3/2\ \pi$ respectively. Matching the

expression (11) with the value of the fluctuating current inside the SOL as given by Eqs. (2-4) yields the required boundary conditions, written here in dimensionless form

$$\frac{\partial}{\partial\theta}\varphi\Big|_{\theta_b} = \pm i\,\alpha\,\varphi|_{\theta_b} \tag{12}$$

where θ_b is $-\pi/2$ and $3/2\ \pi$. The parameter α gives the strength of the sheath current as a response to a fluctuation of the potential. It is given by $\alpha = \alpha_1 \left(k_\theta / k_\perp\right)^2 \left(\omega + i\,\omega_m\right)/\omega_g$, where $\alpha_1 = L_{||}/\sqrt{R x_0}\left(\omega_{pi}^{ed}/k_\theta c\right)^2 \sqrt{T_0/T^{ed}}$ and ω_{pi}^{ed} is the ion plasma frequency at the plasma edge of the sheath.

The eigenvalue problem given by Eq. (8) and boundary conditions (12) can be reduced to a simpler form in some limiting cases. In the low-frequency limit $|\omega| << \omega_m$ perturbations are electrostatic and are described by the following simplified problem

$$\omega \frac{c_A^2}{L_{||}^2}\frac{\partial^2}{\partial\theta^2}\varphi + i\,D_m\left(\omega^2 k_\perp^2 + \omega_g^2 k_\theta^2 \hat{\mathrm{G}}\right)\varphi = 0 \tag{13}$$

$$-\lambda_* \frac{\partial}{\partial\theta}\varphi\Big|_{\theta_b} = \pm\varphi|_{\theta_b} \tag{14}$$

where $\lambda_* = n_0/n^{ed}\sqrt{T^{ed}/T_0}\sqrt{m_i/m_e}\ \lambda / L_{||}$ is a dimensionless form of the electon mean free path λ [4]. Modes described by Eqs. (13)-(14) are known as resistive ballooning modes, since the parallel current density is determined by the Spitzer resistivity of the SOL plasma. The analysis of these modes has been carried out recently by Novakowskii et al. in Ref.[15]. This work shows that strong unstable perturbations, with a growth rate of the same order as ω_g, arise in two different regimes. The first is the so called "strong ballooning" regime. It is characterised by $\omega_m/\omega_g\ \beta_* >> 1$, where $\beta_* = \beta\ L_{||}^2/Rx_0$ is the normalised plasma beta of the ballooning theory. From the physical point of view, this limit arises if either the plasma beta or the poloidal wave number of the perturbation are large. Values of ω_g comparable to γ are expected also in the opposite limit $\omega_m/\omega_g\ \beta_* << 1$ (weakly balloning regime) if the electron mean free path is large, i.e. in the limit $\lambda_* >> 1$.

In order to satisfy the low-frequency requirement leading to the simplified problem given by Eqs. (13)-(14), the condition $\omega_m/|\omega| >> 1$ must be satisfied. Consequently, the fast growing modes described in Ref. [15] arise in the limit $\omega_m/\omega_g >> 1$. This requirement, as will be discussed below, is met only in some limiting cases where the SOL plasma temperature is extremely low. The ratio ω_m/ω_g is given approximately by the following expression, where the SOL temperature T_0 is expressed in eV and lengths are in cm.

$$\frac{\omega_m}{\omega_g} = 4.1 \frac{\Lambda}{10} Z \sqrt{\frac{m_i}{m_p}} \frac{k_\perp^2 \sqrt{R_0 x_0}}{T_0^2} \tag{15}$$

Here Λ is the Coulomb logarithm, m_p is the proton mass, m_i and Z are the ions mass and charge respectively and the numerical factor is due to the parallel Spitzer conductivity. In the framework of the Eikonal approximation of the fluid equations leading to Eq. (8), the inequalities $x_0^{-1} << k_\perp << \rho_s^{-1}$ must be satisfied, where $\rho_s = c_s/\Omega_i$ is the ion Larmor radius. This implies that the following inequalities must hold.

$$\sqrt{\frac{R_0}{x_0^3}} \frac{1}{T_0^2} << \frac{\omega_m}{\omega_g} << \frac{\sqrt{R_0 x_0}}{\rho_s^2} \frac{1}{T_0^2} \tag{16}$$

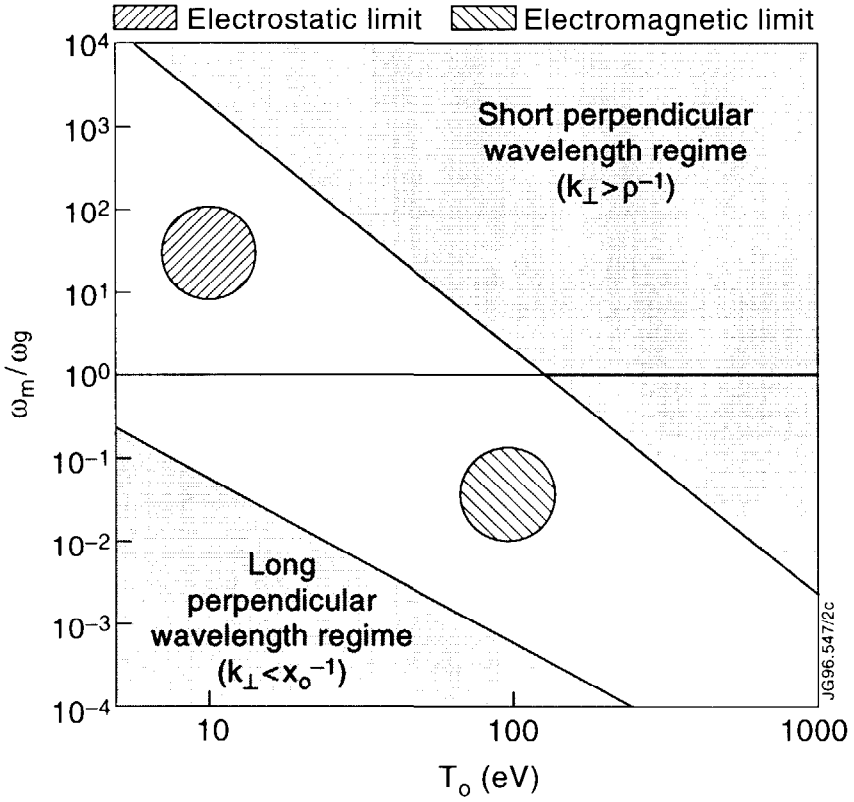

Fig.2: Region of the ω_m / ω_g *space where inequalities (16) are satisfied depending on the equilibrium temperature* T_0 . *Case with* R_0 = 300 cm, x_0 = 2 cm, B = 3 T.

The shaded regions of the diagram indicate regimes where the hypotheses leading to either the fluid equations or the eikonal approximation are not fulfilled. This is due respectively to extremely short or long perpendicular wavelength of the perturbation. The circles show regions where (depending on the perpendicular wavelength and the SOL temperature) perturbations are electrostatic or electromagnetic.

In Fig. 2 is shown the region in the T_0, ω_m/ω_g space where inequalities (16) are satisfied for some characteristic values of R_0, x_0 and of the magnetic field. The electrostatic approximation gives reliable results for SOL temperatures of the order of $T_0 \approx 10$ *eV*,

corresponding to the dotted circle shown in the plot. For SOL temperatures of order $T_0 \approx 100$ eV, which is the order of magnitude of the measured values in many experiments, the opposite limit $\omega_m/\omega_g << 1$ applies (shaded circle in Fig. 2). From the physical point of view, this means that perturbations of the magnetic field cannot be neglected in the fluid equations. The purely electrostatic approach can however be successfully applied to high temperature plasmas in the limit $\lambda_* << 1$, $\beta_* << 1$. In this case the solution of Eqs. (13)-(14) leads to the dispersion relation $\gamma \approx \omega_m \beta_*$ [15]. It corresponds to slow resistive modes described already in Ref. [12] for a different curvature operator.

In the range of frequencies $|\omega| >> \omega_m$ Eqs. (8)-(12) can be recast in the following dimensionless form

$$\frac{\partial}{\partial\theta}\left(\hat{\mathrm{P}}\frac{\partial}{\partial\theta}\right)\varphi + \beta_*\left(-\hat{\mathrm{P}}\Gamma^2 + \hat{\mathrm{G}}\right)\varphi = 0 \tag{17}$$

$$-\frac{\partial}{\partial\theta}\varphi\Big|_{\theta_b} = \pm\frac{\alpha_0}{\hat{\mathrm{P}}}\varphi\Big|_{\theta_b} \tag{18}$$

where $\Gamma = \gamma/\omega_g$ is the dimensionless growth rate, $\hat{\mathrm{P}} = \left(k_\perp/k_\theta\right)^2 = \left[1+\hat{s}^2\left(\theta-\theta_0\right)^2\right]$ and $\alpha_0 = \alpha_1\Gamma$. Modes described by this simplified eigenvalue problem arise when the Spitzer resistivity can be neglected in the SOL region and the current response to an oscillation of the electrostatic potential is determined in the parallel direction by finite sheath conductivity.

Eqs. (17)-(18) have been studied in Ref. [12] for a simplified magnetic geometry, with a step-like curvature operator and neglecting effects due to the shear of the magnetic field lines. Our aim here is to improve the stability analysis by taking into account a more realistic magnetic geometry.

3. ANALYTICAL RESULTS

The aim of this section is to discuss the general properties of the eigenvalue problem given by Eqs. (17)-(18) and to evaluate approximate forms of the dispersion relation in some limiting cases accessible to analytical treatment.

For large values of β_*, Eqs. (17)-(18) describe a fast growing (ideal) perturbation with Γ of order unity. Ideal modes are not affected by the value of the sheath conductivity. If however α_0 is large, they become stable when β_* is below a critical threshold β_{cr}. The evaluation of β_{cr} by means of numerical techniques is discussed in the following section. Here we are interested in the description of the modes due to finite sheath conductivity, which are relevant when β_* is below the critical threshold.

A solution of the eigenvalue problem given by Eqs. (17)-(18) satisfies the Euler-Lagrange principle $\delta E = 0$, where the energy functional E is given by the following expression (prime denotes a θ derivative).

$$E = \alpha_0 \left(\left| \varphi \right|_{3/2\,\pi}^2 + \left| \varphi \right|_{-\pi/2}^2 \right) + \int_{-\pi/2}^{3/2\,\pi} \left[\hat{\mathrm{P}} \left| \varphi' \right|^2 - \beta_* \left(-\hat{\mathrm{P}} \Gamma^2 + \hat{\mathrm{G}} \right) \left| \varphi \right|^2 \right] d\theta \tag{19}$$

A variational method can be used to derive an approximated dispersion relation. Basically the technique consists of two steps. First, a one-parameter family of functions $\varphi_c(\theta)$ (trial functions) is chosen, such that any function of the family approximately satisfies Eqs. (17)-(18). The value of the parameter which gives the best approximation is evaluated imposing the minimum condition $\partial E / \partial c = 0$. The dispersion relation is then given by $E = 0$, where E is computed by means of the best trial function.

The following part of this section is devoted to the application of the technique outlined above. In order to perform an analytical treatment of the problem we take the limit $\beta_* << \beta_{cr}$, $\Gamma << 1$, which allows us to neglect terms of order Γ^2 in Eqs. (17) and (19). In this limit the eigenvalue of the problem becomes α_0 and the growth rate is determined as

$$\Gamma = \frac{\alpha_0}{\alpha_1} = \alpha_0 \frac{\sqrt{R x_0}}{L_{\|}} \left(\frac{k_\theta c}{\omega_{pi}^{ed}} \right)^2 \sqrt{\frac{T^{ed}}{T_0}} \tag{20}$$

Two different families of trial functions are required in order to solve the eigenvalue problem in the asymptotic limit $\beta_* \to 0$ and when β_* is small, but finite. In the first case the perturbations are flute-like. If $\beta_* = 0$ Eqs. (17)-(18) have the trivial solution $\varphi = const$, $\alpha_0 = 0$. A trial function family can therefore be written as $\varphi_c(\theta) = 1 + c\, f(\theta)$, where $c << 1$ and f is the asymmetric part of the eigenfunction. The minimum condition gives

$$c = \beta_* \frac{\int_{-\pi/2}^{3/2\,\pi} \hat{\mathrm{G}} f \, d\theta}{\int_{-\pi/2}^{3/2\,\pi} \hat{\mathrm{P}} \left| f' \right|^2 d\theta - \beta_* \int_{-\pi/2}^{3/2\,\pi} \hat{\mathrm{G}} \left| f \right|^2 d\theta} \tag{21}$$

so that the approximated dispersion relation reads

$$\alpha_0 = \tfrac{1}{2} \beta_*^2 \frac{\left(\int_{-\pi/2}^{3/2\,\pi} \hat{\mathrm{G}} f \, d\theta \right)^2}{\int_{-\pi/2}^{3/2\,\pi} \hat{\mathrm{P}} \left| f' \right|^2 d\theta - \beta_* \int_{-\pi/2}^{3/2\,\pi} \hat{\mathrm{G}} \left| f \right|^2 d\theta} \tag{22}$$

These results allow us to draw some preliminary conclusions, independently from the analytical form of f. First of all, the growth rate of the modes has a quadratic dependence on β_* in the limit $\beta_* \to 0$. This is due, as shown in Ref. [12], to the fact that a line of force lies partly in the destabilising curvature region ($\theta > \pi/2$) and partly in the stabilising region ($\theta < \pi/2$).

Consequently, flute-like perturbations cannot display strong unstable behaviour. Furthermore Eqs. (21) and (22) show that in general c and α_0 may display singularities for some values of β_*, leading to the failure of the hypotheses $c << 1$ and $\Gamma << 1$. Based on this consideration, we shall refer to a trial function non belonging to the restricted class $\varphi = 1 + cf$ (with $c << 1$) in the small but finite β_* case, so that non flute-like (and consequently strongly unstable) modes can be accurately modelled.

The analytical form of the trial function to be inserted in Eqs.(21)-(22) is derived from the following approximated general solution of Eq. (17)

$$\varphi = \left[A + B \arctan\left(\hat{s}\left(\theta - \theta_0\right)\right)\right]\left(1 + \beta_* \frac{\hat{G}}{\hat{P}}\right) \tag{23}$$

where A and B are arbitrary constants. Rel. (23) has been obtained by means of the asymptotic technique outlined in the appendix.

Expression (23) is not suitable to be adopted as a trial function without further simplifications. In the small shear limit we neglect the second term in the square bracket. The asymmetric part of the solution is then entirely determined by the term proportional to the curvature operator. Consequently, an appropriate trial function reads $\varphi = 1 - c\cos\theta$. On the other hand, we retain only the terms in the square bracket of Rel. (23) in the opposite limit $\hat{s} >> 1$. The required trial function in this case is given by $\varphi = 1 + c \arctan\left[\hat{s}\left(\theta - \theta_0\right)\right]$.

The dispersion relation (22) is evaluated explicitly in the case of both small and large shear. In leading order in β_* it reads

$$\alpha_0 \approx 2\pi\beta_*^2 \qquad \hat{s} << 1 \tag{24}$$

$$\alpha_0 \approx 8\pi\beta_*^2\hat{s} \qquad \hat{s} >> 1 \tag{25}$$

In the finite β_* case the flute-like trial functions used in the evaluation of Eq. (24)-(25) with $c << 1$ are no longer adequate for an analytical treatment of the problem. Since, in the small β_* limit, the asymmetric part of the eigenfunction is proportional to β_* itself, a suitable form of the trial function in the finite beta, large shear case is given by

$$\varphi_c = \frac{1}{2} + \frac{1}{\pi}\arctan\left[\hat{s}\left(\theta - \theta_0\right)\right] + c \tag{26}$$

Conditions $E=0$ and $\partial E/\partial c = 0$ give a nonlinear system in the unknown quantities c and α_0. It can be easily solved in the $\hat{s} >> 1$ limit, where the trial function (26) is step-like. In this case the solution reads

$$\alpha_0 \approx 16\,\pi\beta_*^2 \frac{\left(\hat{s}+1\right)^2}{\sqrt{\hat{s}^2 + 16\,\pi^2\,\beta_*^2\left(\hat{s}+1\right)^2} + \hat{s}} \tag{27}$$

This latter approximation of the dispersion relation is consistent with Rel. (25) in the $\beta_* \rightarrow 0$ limit. If the condition $16\pi^2 \beta_*^2 >> 1$ is satisfied, Rel. (27) can be recast in the following simpler form

$$\alpha_0 \approx 4\beta_* (\hat{s}+1) \tag{28}$$

Expression (28) can be compared with the dispersion relation given in Ref. [12] in the $\beta_* << \beta_{cr}$ limit for modes localised on the low field side of the torus in a double-null divertor configuration. Both relations display a linear dependence of the growth rate on the normalised beta. We stress that in a double-null configuration the linear dependence is related to the asymmetry of the curvature operator in Eq. (17), due to the peculiar vacuum magnetic field configuration. Here the same dependence is related to the strong asymmetry of the eigenfunction which, as a consequence of the finite magnetic shear, is mainly localised in the unfavourable curvature region. This effect screens the different results arising from the stability analysis of single- and double-null configurations.

4. NUMERICAL ANALYSIS

In this section the analytical dispersion relations derived above are compared with the numerical solution of the problem given by Eq. (17) and boundary conditions (18). Following a well established technique [20], Eq. (17) is recast in a system of three first order ODE (the third dependent variable being the eigenvalue). Boundary conditions (18) are satisfied solving the system with a shooting method. According to the ballooning mode theory, the growth rate is then maximised by varying θ_0, at fixed values of β_*, α_I and $\hat{s}$.

Numerical simulations allow a check of the accuracy of the approximations made in the previous section. They also show how modes due to finite sheath conductivity, characterised by $\gamma << \omega_g$, develop into ideal modes (with $\gamma \approx \omega_g$) when the normalised plasma beta increases.

The threshold value β_{cr} for the onset of ideal modes can be evaluated as the value of β_* where the growth rate of the modes becomes positive in the limit $\alpha_0 \rightarrow \infty$ (lines of force frozen into the sheath). Since this limiting case is not accessible to the numerical analysis with boundary conditions (18), Eq. (17) has been solved for this purpose with boundary conditions $\varphi = 0$ at $\theta = -\pi/2$ and $\theta = 3/2\ \pi$. The stability diagram for ideal modes in the β_*, $\hat{s}$ space is shown in Fig. 3. For large $\hat{s}$ values, the diagram shows the stabilising effect of the magnetic shear, with $\beta_{cr} \approx \hat{s}/2$, as it is well known from the ballooning mode theory inside the magnetic separatrix.

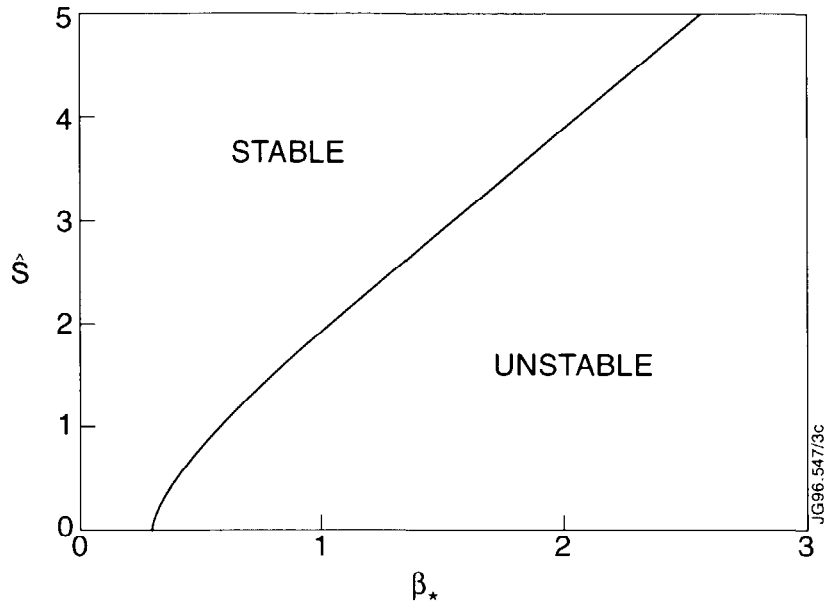

Fig.3: Stability diagram for ideal modes.

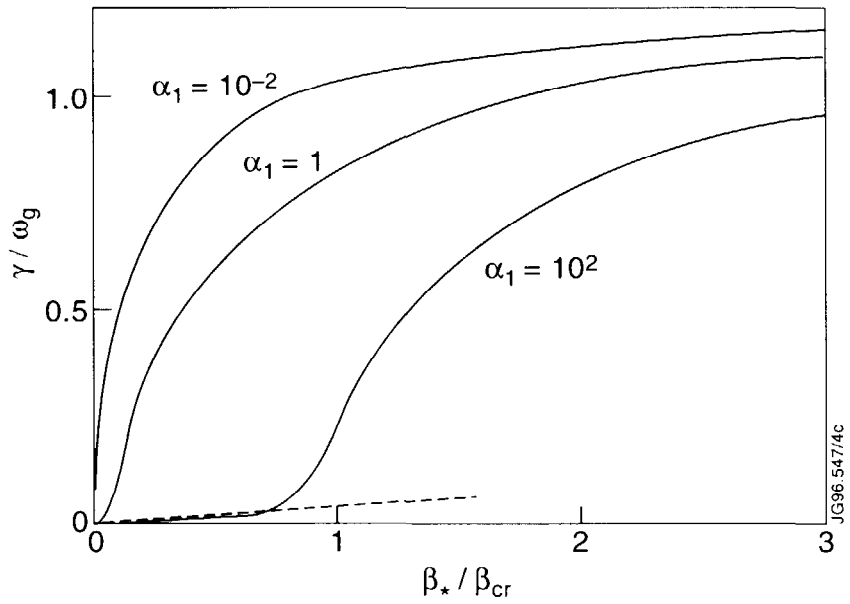

Fig.4: Solid curves: normalised growth rate in the case $\hat{s} = 1$, *plotted versus* β_* / β_{cr} *for different values of the sheath conductivity. Lines of force are frozen into the sheath if* $\alpha_1 \to \infty$ *and completely unfrozen if* $\alpha_1 \to 0$. *Dashed line: analytical approximation Rel. (28) for* $\alpha_1 = 10^2$.

In the regime where the sheath resistivity becomes important, we first consider the case $\hat{s} = 1$. In Fig. 4 the normalised growth rate is plotted versus β_* for three characteristic values of α_1 . For $\beta_* > \beta_{cr}$, the modes are not dramatically affected by the sheath conductivity, as discussed above, while it becomes the key parameter if β_* lies below the critical threshold. In fact, modes in this region are stable in the limit $\alpha_1 \to \infty$ and they become more and more unstable as α_1 decreases. In the limit $\alpha_1 << 1$ (lines of force completely unfrozen), the growth

rate is of order ω_g even if β_* lies well below the threshold value. This is consistent with our theoretical estimate Eq. (20). We stress that, although in this limit electrostatic resistive modes are not considered, the instability arises for any value of β_* due to the finite sheath conductivity. The dependence of the growth rate on the normalised beta is quadratic in the limit $\beta_* \to 0$ for any value of α_I, consistently with our approximate results (24)-(25). For very small values of α_I, however, the region of quadratic dependence along the β_* axis is very close to zero and is not resolved in Fig. 4. When α_I is large the condition $\gamma << \omega_g$ is met at values of the normalised beta of order unity. Consequently, relation (28) can be compared with the numerical values. The dashed line in Fig. 4 shows the normalised growth rate computed by means of the linear approximation (28), in very good agreement with the numerical value.

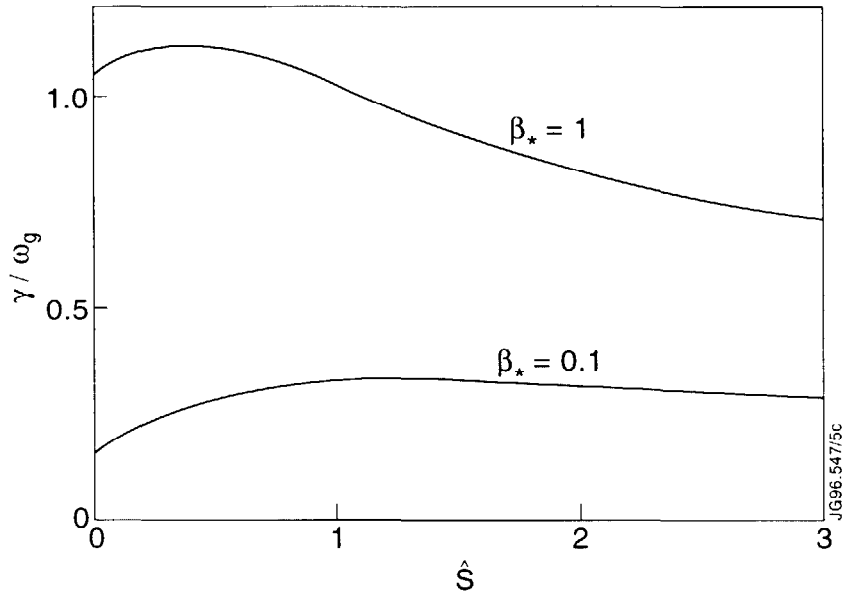

Fig.5: Normalised growth rate in the case $\alpha_1 = 1$, *plotted versus* $\hat{s}$ *for different values of* β_*.

The shear dependence of the growth rate is analysed next. The results are displayed in Fig. 5 for two different values of the normalised plasma beta. For large values of β_* the modes are stabilised by the magnetic shear, as it enhances the threshold for the onset of the ideal instability. On the other hand, $\hat{s}$ shows a destabilising effect at values of β_* smaller than β_{cr}. This is a consequence of the fact that, except for the $\theta_0 = \pi/2$ case, the curvature operator is not in general an odd function of the poloidal angle for finite $\hat{s}$ values (parity is actually assessed by symmetry around $\theta = \pi/2$ i.e. the top of the cross-section in Fig. 1). Since then stabilising and destabilising effects of the curvature do not balance, even perturbations not strongly localised in the outer region of the torus (as in the small β_* case) may have finite growth rate. This is consistent with our approximate results (27)-(28). The combined stabilising and destabilising influence of the magnetic shear determines a maximum of the growth rate at values of $\hat{s}$ of order unity.

The numerical analysis is completed by a discussion of the properties of the eigenfunctions corresponding to the different cases discussed. In Fig. 6 three characteristic eigenfunctions are plotted for comparison. The first corresponds to a case with $\beta_* >> \beta_{cr}$ and $\gamma \approx \omega_g$. It shows the typical feature of an ideal mode: it is close to zero at the boundary $\theta=-\pi/2$ and it is located mainly in the outer region of the torus ($\theta > \pi/2$), where the curvature operator of Eq. (17) has a destabilising effect. The second is a flute-like perturbation. It corresponds to a case where β_* is very small and $\gamma \approx \beta_*{}^2\, \omega_g$. It displays the characteristic behaviour of the trial function used in order to derive the approximate relation (25). The third eigenfunction is an example of what we refer to as the small but finite β_* case. It corresponds to a situation where β_* is below the ideal threshold, magnetic shear is large and $\gamma \approx \beta_*\ \omega_g$. This eigenfunction resembles the step-like trial function (26), used in the derivation of the approximate dispersion relation (27).

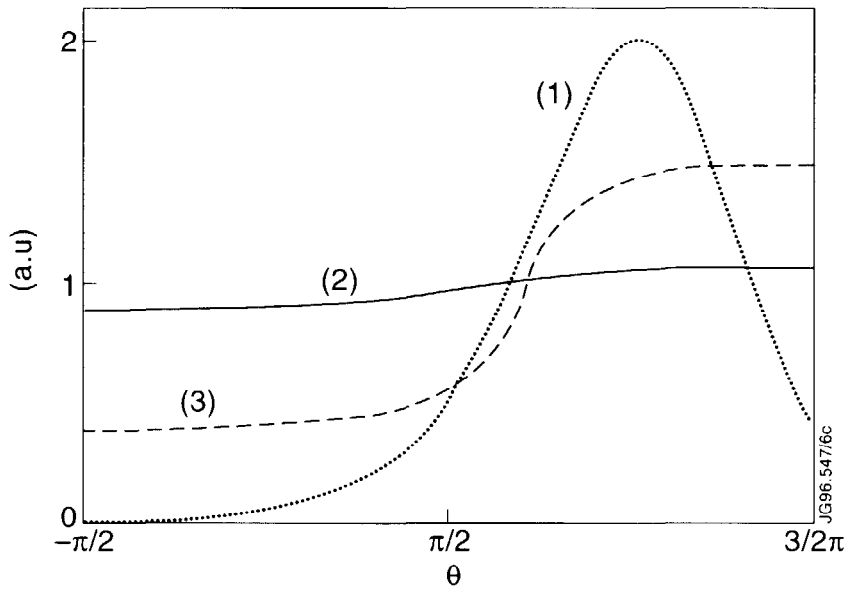

Fig.6: The eigenfunction structure. Case (1) represent an ideal ballooning mode, case (2) is a flute-like perturbation and case (3) arise when the plasma beta is not strong enough to shift the perturbation in the unstable curvature region, but the eigenfunction is asymmetric as a consequence of the finite magnetic shear.

(1)	$\beta_* = 3\ \beta_{cr}$;	$\hat{s} = 1$;	$\alpha_1 = 10$;	$\gamma = 0.98\ \omega_g$;	$\theta_0 = 3.14$
(2)	$\beta_* = 2 \times 10^{-2}\ \beta_{cr}$;	$\hat{s} = 1$;	$\alpha_1 = 1$;	$\gamma = 7 \times 10^{-3}\ \omega_g$;	$\theta_0 = 1.59$
(3)	$\beta_* = 6.7 \times 10^{-2}\ \beta_{cr}$;	$\hat{s} = 3$;	$\alpha_1 = 1$;	$\gamma = 0.28\ \omega_g$;	$\theta_0 = 2.11$

Finally, in Fig. 7 the value of the origin of the perturbation θ_0 where the growth rate has its maximum is displayed versus the normalised beta, at fixed values of the sheath conductivity and magnetic shear. At values of β_* below the ideal threshold the eigenfunction is mostly determined by the sheath physics through the boundary conditions. Consequently, θ_0 lies halfway between the end plates (corresponding to $\theta = \pi/2$). When the normalised beta is close

and above the ideal threshold, the ideal instability sets in and θ_0 moves toward the outer mid plane of the torus, corresponding to $\theta = \pi$.

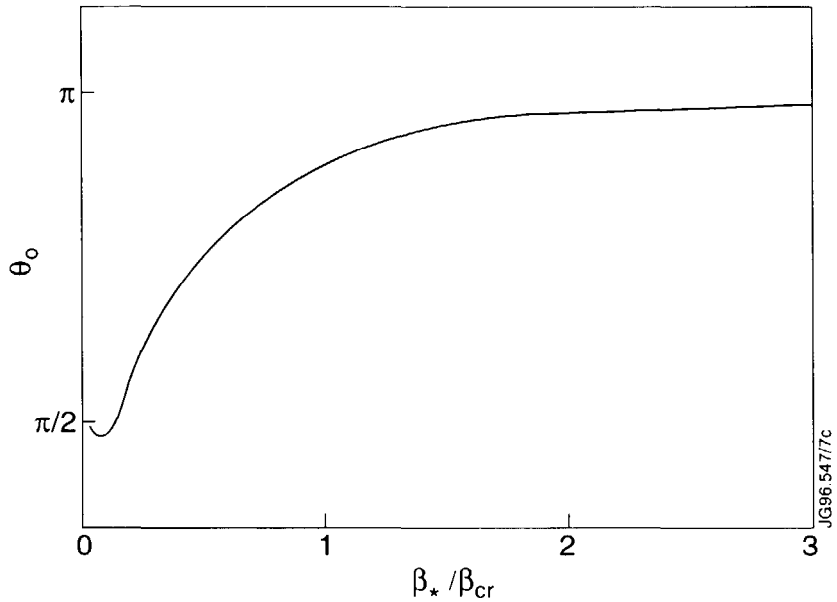

Fig.7: Dependence of θ_0 *from* β_* / β_{cr}. *Case with* $\hat{s} = 1$, $\alpha_1 = 1$.

5. DISCUSSION

In this paper we have carried out a stability analysis of modes driven by combined pressure gradient and unfavourable curvature in SOL plasmas. The work has mainly been devoted to the study of the dependence of the growth rate on the conductivity of the Debye sheath close to the end plates. A similar problem has been studied in the electrostatic limit in Ref. [15]. Our analysis is based on an electromagnetic model and yields substantial new results.

First of all we studied the problem at values of beta normalised much smaller than the ideal critical threshold value, by means of analytical techniques (in section 3) and a numerical technique (in section 4). In this limit the growth rate of electrostatic perturbations is determined by the electron mean free path, leading to finite Spitzer conductivity of the SOL. Our analysis showed that the stability of electromagnetic modes is determined by the finite Debye sheath conductivity. We found that the key parameter governing the instability is α_1, which is mainly determined by the density of charged particles inside the sheath. The growth rate is related to the SOL and sheath temperatures T_0 and T^{ed} as well, but this dependence plays a less critical role than in the electrostatic model. As a consequence, an electromagnetic instability at low beta can arise also in the collisionless limit.

At high values of the normalised pressure gradient β_*, but still lower than the ideal threshold, resistive modes smoothly transform into ideal modes, which are only slightly affected by the sheath conductivity. This transition, which cannot be described in the

framework of an electrostatic model, has been analysed numerically in section 4. In particular, we have considered the influence of the shear of the magnetic lines of force on the growth rate. We showed that it has a stabilising effect on ideal modes, as for balloning modes inside the last closed flux surface. On the other hand, at small values of β_*, it can lead to an enhancement of the growth rate.

Our results can be applied to a tokamak plasma with a poloidal single-null divertor configuration. The analysis gives some insight into the dependence of the growth rate on β_*, as discussed in section 3. The presence of a X-point in the poloidal magnetic field leads however to a dramatic enhancement of the length of the lines of force and of the magnetic shear in the region close to the X-point itself. Consequently, an accurate description of the interchange instability in a divertor configuration requires further investigations.

ACKNOWLEDGEMENTS

One of the authors (A.N.) is grateful to the JET Joint Undertaking for its hospitality and support during the performance of this work.

APPENDIX:
AVERAGING METHOD FOR THE SOLUTION OF ODE

A method for solving Eq. (17), which is a second order linear ODE with non constant coefficients, is discussed here. Since accurate analytical solutions of Eq. (17) are unknown, we shall refer to a technique of approximate solution developed by Bogolyubov, known as the method of averaging. A brief derivation of the basic formulas is outlined in Ref. [21] and the method has been applied to the ballooning mode investigation by one of the authors together with Yurchenko in Ref. [18].

We exploit the fact that in the limit $\hat{s} << 1$ the coefficients of Eq. (17) exhibit both a slow non periodic dependence on the poloidal angle over an interval of length $1/\hat{s}$ and a fast oscillatory behaviour due to the presence of the curvature operator $\hat{G}$. In order to combine the two different scales of the problem we introduce the slow variable $t = \hat{s}\,(\theta-\theta_0)$.

By the substitution $\varphi = y/\sqrt{\hat{P}}$ Eq. (17) is recast into a Schrödinger-type equation

$$\frac{d^2y}{dt^2} - V\,y = 0 \tag{A1}$$

where the effective potential is

$$V = \frac{\hat{s}^2}{\sqrt{1+t^2}}\frac{d^2}{dt^2}\sqrt{1+t^2} + \frac{\beta_*}{\hat{s}^2}\left(\Gamma^2 + 2\frac{t\sin\theta + \cos\theta}{1+t^2}\right) \tag{A2}$$

The potential (A2) is a slowly changing well with rapid oscillations superimposed. We average it over a fast period. Slowly and rapidly changing parts are introduced

$$\overline{V} = \frac{1}{2\pi}\int_0^{2\pi} V(t,\theta)d\theta \tag{A3}$$

$$\tilde{V} = V - \overline{V} \tag{A4}$$

In the same way the solution of the problem is split into a slow and an oscillatory part

$$y = \overline{y}(t) + \tilde{y}(t,\theta) \tag{A5}$$

The slow solution satisfies a differential equation analogous to Eq. (A1)

$$\frac{d^2\overline{y}}{dt^2} - \langle V\rangle\overline{y} = 0 \tag{A6}$$

where the modified potential $\langle V \rangle$ can be expressed by a series in the smallness parameter $\hat{s}$. Up to second order in $\hat{s}$ it reads

$$\langle V \rangle = \frac{\hat{s}^2}{\left(1+t^2\right)^2} + \beta_* \Gamma^2 - 2\frac{\beta_*^2}{1+t^2} \tag{A7}$$

The oscillatory part of the solution turns out to be fully determined by the slow part. It satisfies the following equation

$$\frac{d^2\tilde{y}}{d\theta^2} - \tilde{V}\bar{y} = 0 \tag{A8}$$

Up to second order in $\hat{s}$ Eq. (A8) is easily solved by successive integrations leading to

$$\tilde{y} = -2\beta_* \frac{t\sin\theta + \cos\theta}{1+t^2}\bar{y} \tag{A9}$$

Eq. (A6) cannot be solved analytically for the potential (A7), indicating that so far we took no advantage of the application of the averaging method. Neglecting terms of order Γ^2 and β_*^2 in the modified potential (A7) however, the averaged equation (A6) coincides with the starting equation (A1) in the case $\beta_* = 0$, which admits an exact general solution

$$\bar{y} = \sqrt{1+t^2}\left(A + B\arctan t\right) \tag{A10}$$

where A and B are arbitrary constants. Inserting this latter result into relation (A9) allows to evaluate the oscillatory part of the general solution of Eq. (A1) to the same accuracy in β_*. The general solution of Eq. (17) to first order in β_* reads therefore (Cf. Eq. (23))

$$\varphi = \left(A + B\arctan t\right)\left(1 - 2\beta_* \frac{t\sin\theta + \cos\theta}{1+t^2}\right) \tag{A11}$$

REFERENCES

[1] V.K. Kolesnikov and A.V. Nedospasov, Sov. Phys. Dokl. **32**, 478 (1987)

[2] A.V. Nedospasov, Sov. J. Plasma Phys. **15**, 659 (1989)

[3] X. Garbet, L. Laurent, J.-P. Roubin, A. Samain, Nucl. Fusion **31**, 967 (1991)

[4] A.V. Nedospasov, Phys. Fluids B **5**, 3191 (1993)

[5] A.V. Nedospasov, D.A. Uzdensky, Contrib. Plasma Phys. **34**, 277 (1994)

[6] H.L. Berk, D.D. Ryutov and Yu.A. Tsidulko, JETP Lett. **52**, 23 (1990)

[7] H.L. Berk, D.D. Ryutov and Yu.A. Tsidulko, Phys. Fluids B **3**, 1346 (1991)

[8] H.L. Berk, R.H. Cohen, D.D. Ryutov, Yu.A. Tsidulko, X.Q. Xu, Nucl. Fusion. **33**, 263 (1993)

[9] X.Q. Xu and R.H. Cohen, Plasma Phys. Control. Fusion. **35**, 1071 (1993)

[10] N.N. Kukharkin, M.V. Osipenko, O.P. Pogutse, V.M. Gribkov, in *Plasma Physics and Controlled Nuclear Fusion Research 1992* (Proc. 14th Int. Conf. Würzburg, 1992) Vol. 2, IAEA, Vienna, p.293

[11] O.Pogutse, W. Kerner, in *Proc. 21st EPS Conf. On Controlled Fusion and Plasma Phys.* (Montpellier, 1994) Vol. 1, p. 99

[12] O.Pogutse, W. Kerner, *The SOL Width and MHD Interchange Instability in Tokamaks*, JET-P(94) 44

[13] W. Kerner, O.Pogutse, R. Van der Linden, B. Schnuke, *ELMs as Ideal Interchange Instabilities near the Separatrix*, JET-P(96) 17

[14] J.G. Cordey, W. Kerner, O.Pogutse, A. Nassigh, *On the dependence of the L-H Power Threshold on the Ion Drift Direction*, JET-P(96) 09

[15] S.V. Novakovskii, P.N. Guzdar, J.F. Drake and C.S. Liu, Phys. Plasmas **2**, 3764 (1995)

[16] B.B. Kadomtsev and O.P. Pogutse, Sov. Phys.-JETP **38**, 283 (1974)

[17] H.R. Strauss, Phys. Fluids **19**, 134 (1976)

[18] O.P. Pogutse and E.I. Yurchenko, in *Reviews of Plasma Physics*, Vol. 11, Consultants Bureau (New York 1965)

[19] J.W. Connor, R.J. Hastie and J.B. Taylor, Proc. R. Soc. Lond. A. **365**,1 (1979)

[20] W.H. Press, B.P. Flannery, S.A. Teukolski, W.T. Vetterling, *Numerical Recipes,* Cambridge University Press (Cambridge 1989)

[21] A.I. Morozov and L.S. Solov'ev, in *Reviews of Plasma Physics*, Vol. 2, Consultants Bureau (New York 1966)